Nanoparticle-induced surface reconstruction of phospholipid membranes

Bo Wang[a], Liangfang Zhang[b], Sung Chul Bae[a], and Steve Granick[a,b,c,d,1]

Departments of [a]Materials Science and Engineering, [b]Chemical and Biomolecular Engineering, [c]Chemistry, and [d]Physics University of Illinois, Urbana IL 61801

Edited by Nicholas J. Turro, Columbia University, New York, NY, and approved October 8, 2008 (received for review July 27, 2008)

The nonspecific adsorption of charged nanoparticles onto single-component phospholipid bilayers bearing phosphocholine headgroups is shown, from fluorescence and calorimetry experiments, to cause surface reconstruction at the points where nanoparticles adsorb. Nanoparticles of negative charge induce local gelation in otherwise fluid bilayers; nanoparticles of positive charge induce otherwise gelled membranes to fluidize locally. Through this mechanism, the phase state deviates from the nominal phase transition temperature by tens of degrees. This work generalizes the notions of environmentally induced surface reconstruction, prominent in metals and semiconductors. Bearing in mind that chemical composition in these single-component lipid bilayers is the same everywhere, this offers a mechanism to generate patchy functional properties in phospholipid membranes.

fluorescence | adsorption | phase transition

That phospholipid membranes possess patchy functional properties (different from spot to spot) is fundamental to their use as biomaterials and biosensors (1, 2) as well as abundant cellular activity (3–6). The extensive and sometimes contentious literature on the origins of spatial modulation supposes patchiness to arise from inhomogeneous distribution of the different lipids and other components within typical membranes and, in some cases, to specific binding (7–10). Here, phospholipid vesicles that do not satisfy the traditional requirements are stimulated to display spatial patchiness in response to nonspecific binding by charged nanoparticles. By using fluorescence and calorimetry methods to study membranes formed from single-component lipids with phosphocholine head groups, anionic nanoparticles are shown to induce local gelation in otherwise fluid bilayers and cationic nanoparticles to induce local fluidization of otherwise gelled bilayers. This work generalizes the notions of environmentally induced surface reconstruction, prominent in metals and semiconductors (11–13); however, unlike adsorption-induced surface restructuring of solids, the present systems are more strongly influenced by the high mobility of the lipid molecules that comprise phospholipid membranes. It also suggests origins of potential biological activity of nanoparticles that increasingly are exposed through the environment to living systems by accident and design (14, 15).

The hypothesis that motivates this study is summarized in Fig. 1: A phospholipid bilayer's local phase state can be switched by binding of charged nanoparticles such that they alter the tilt angle of the phosphocholine (PC) head group, which is terminated by an electric dipole of phosphate and choline, P^-–N^+. Negatively charged (anionic) nanoparticles interact preferentially with the N^+ terminus, raising the angle of the dipole above the average angle of 0° to ≈3° characteristic of the fluid phase (16) and recruiting lipid tails to increase in density; conversely, positively charged (cationic) nanoparticles reduce the tilt angle below the angle of 30° to ≈65° characteristic of the gel phase (16), stimulating a reduced lipid density. To exclude the traditional explanations of spatial patchiness based on specific binding, redistribution of membrane components, and phase separation between different lipids (7–10), these possibilities were eliminated by constructing phospholipid membranes comprised of a sole lipid type. The possibility of specific binding was eliminated by selecting lipids bearing phosphocholine head groups, which are uncharged under the buffer conditions of these experiments (17).

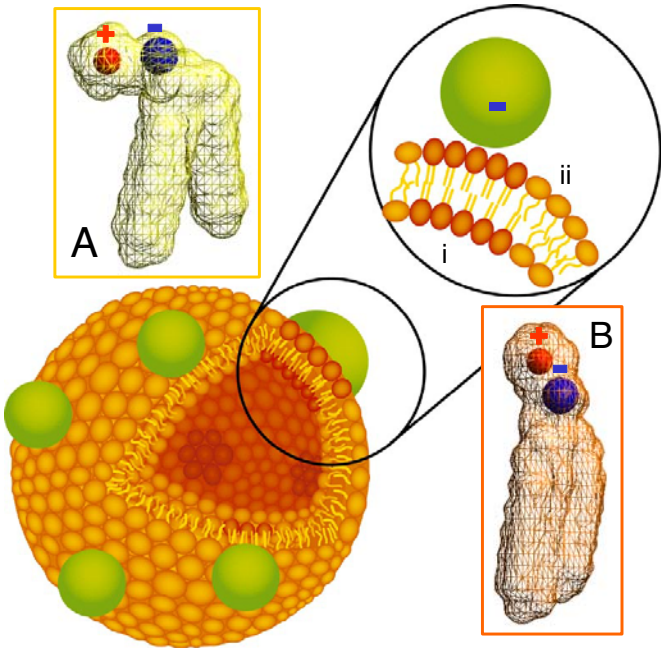

Fig. 1. Schematic diagram of a phospholipid bilayer vesicle with bound nanoparticles. Binding of anionic nanoparticles to a lipid bilayer in the fluid phase causes the nanoparticle to template a gel phase in the place where the nanoparticle binds. Binding-induced reorientation of the phosphocholine (PC) head group causes lipids in the fluid phase to have lower density (*A*) than in the gel phase (*B*). In the PC head group, P^- and N^+ are denoted by blue and red, respectively.

The phospholipids used here, DOPC (dioleoyl PC), DLPC (dilauryl PC), and DPPC (dipalmitoyl PC), have a gel-to-fluid phase transition temperature (T_m) of approximately −20 °C, approximately −1 °C, and approximately +40 °C, respectively. Large unilamellar lipid vesicles (liposomes) were prepared at 1 vol% concentration in PBS buffer (10 mM; pH, 6.0) by the well-known extrusion method. The main nanoparticles used were carboxyl-modified (negatively charged; ≈0.91 e^-/nm^2) and

Author contributions: B.W., L.Z., and S.G. designed research; B.W. performed research; L.Z., S.C.B., and S.G. analyzed data; and B.W. and S.G. wrote the paper.

The authors declare no conflict of interest.

This article is a PNAS Direct Submission.

[1]To whom correspondence should be addressed. E-mail: sgranick@uiuc.edu.

This article contains supporting information online at www.pnas.org/cgi/content/full/0807296105/DCSupplemental.

amidine-modified (positively charged; ≈0.25 e^+/nm^2) white polystyrene (PS) latex with a diameter of 20 nm; in control experiments, silicon dioxide nanoparticles (≈0.11 e^-/nm^2) and supercoiled plasmids were also used. Charged nanoparticles were mixed by vortex into the liposome suspension at the desired molar ratio (18). Measurements were performed at room temperature. It is known that charged nanoparticles, both anionic and cationic, adsorb to the PC group of phospholipids and that liposomes carrying adsorbed nanoparticles maintain their integrity as discrete liposomes (18, 19).

A simple initial test of our hypothesis was that adsorption by anionic nanoparticles should cause liposomes to shrink because the area per lipid head group is less in the gel than in the fluid phase. The anticipated shrinkage of initially fluid liposomes when anionic nanoparticles adsorb was confirmed, showing shrinkage by ≈20% [see supporting information (SI) *Text*]. A delicate point then became to decide whether phase-separated regions would clump together; the tendency to minimize line tension favors this, but electrostatic repulsion between charged nanoparticles resists it. Electron microscopy was not successful in imaging the spatial distribution of nanoparticles, their binding to liposomes being too weak to survive quench to the needed cryogenic temperatures. However, fluorescence imaging at room temperature revealed a highly dynamic spatial distribution and no aggregation of the nanoparticles on optical length scales when they adsorbed to giant unilamellar vesicles (GUVs). Förster resonance energy transfer (FRET) experiments described below set an even smaller upper bound on the size of phase-separated regions, 10–100 nm.

Moving to information on a molecular level, Fig. 2*A* illustrates the raw fluorescence data when anionic nanoparticles were allowed to bind to DLPC liposomes containing embedded Laurdan, which is an uncharged fluorescent dye whose emission is known to be diagnostic of a phospholipid membrane's phase state (20). Normally, Laurdan assay is used to diagnose a membrane's phase when temperature is varied; this work is considered an application to diagnose surface reconstruction. Fluorescence emission is plotted against wavelength, and one observes the progressive rise of blue emission and loss of red emission as nanoparticle concentration increased—suggestive of fluid–gel phase coexistence such that the proportion of fluid to gel phase varies. For quantification, emission intensity was compared at the wavelengths of peak emission intensity for bilayers in pure fluid and gel phases. Fig. 2*B* plots against normalized nanoparticle concentration the intensity fraction of these 2 peaks, and one sees that the changes are linear over a considerable span of nanoparticle concentration. Their normalized difference is the traditional definition of the net polarization, $P \equiv (I_B - I_R)/(I_B + I_R)$, where I_B and I_R are the emitted intensity at these wavelengths in the blue and red, respectively (20). From the data in Fig. 2*B*, *P* was calculated and found to vary smoothly between values characteristic of the membrane fluid phase (no added nanoparticles) and the gel phase (maximum concentration of added nanoparticles). The proportionality to nanoparticle concentration signifies that nanoparticles bound in proportion to their concentration in the environment and that lipid gelled in local spots where nanoparticles bound. Fig. 2*C* plots the implied lipid gel fraction against surface coverage.

The findings did not depend on choice of the lipid: The data are the same when the same anionic nanoparticles were allowed to bind to DOPC liposomes, whose T_m is approximately −20 °C. The findings did not depend on liposome size either, being indistinguishable for liposomes 200 and 80 nm in mean diameter. Silica particles had a similar but weaker effect (data not shown) but presented the advantage of offering a range of particles of different size but similar chemical makeup. These experiments demonstrated that the nanoparticle size plays a minor role. The density of surface charge on the nanoparticles, nearly an order

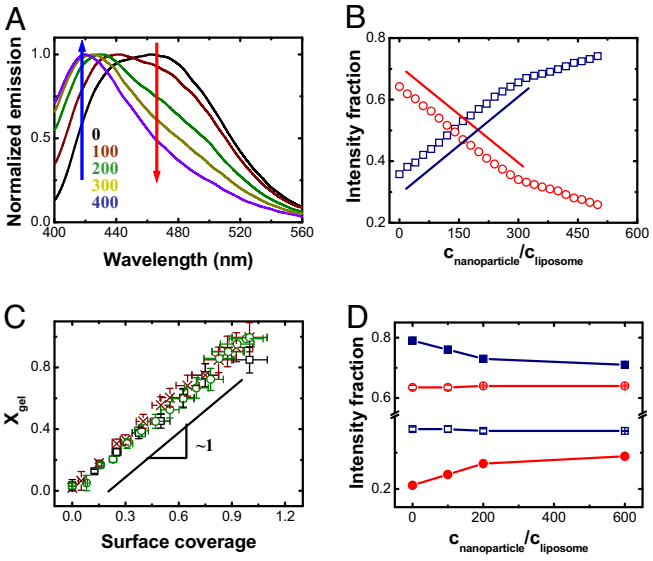

Fig. 2. Experiments in which the fluorescence spectrum of Laurdan, an uncharged fluorescent dye that segregates into the hydrophobic region of lipid bilayers, is used to indicate the membrane phase state. (*A*) Normalized emission plotted against wavelength after anionic (carboxyl-modified) nanoparticles bind to 200-nm DLPC liposomes. The plot compares the cases of number ratio of particles to liposomes C_{NP}/C_L = 0, 100, 200, 300, and 400. (*B*) From data of the kind illustrated in *A*, the intensity fraction of blue and red emission at 416 (blue) and 473 nm (red) is plotted against C_{NP}/C_L. Lines with slope of unity are drawn for comparison. (*C*) Mole fraction of gel phase plotted against surface coverage for binding of anionic nanoparticles onto 200-nm fluid DLPC liposomes (red), 200-nm fluid DOPC liposomes (black), and 80-nm fluid DLPC liposomes (green); the data coincide within experimental uncertainty. (*D*) The intensity fraction of blue emission (416 and 440 nm for DLPC and DPPC, respectively) and red emission (473 and 490 nm for DLPC and DPPC, respectively), plotted against C_{NP}/C_L for binding of cationic (amidine-modified) nanoparticles onto liposomes of DLPC (open symbols) and DPPC (filled symbols).

of magnitude larger for carboxyl-modified polystyrene latex than for silica, correlates with the stronger enhancement of the phase transition that was observed for carboxyl-modified latex. All these nanoparticle systems share the feature that charge on these objects was held rigidly in place. Adsorbed DNA, which also is anionic, did not produce this effect. We believe the reason to be that whereas DNA is flexible, the rigidity of charge placement on nanoparticles enables them to template the phase state of the phospholipids to which they bind. This null result for the case of flexible charged objects incidentally demonstrates that the photophysical response of the fluorescent dye was unmodified by charge, thus validating the data in Fig. 2.

The hypothesis of this article predicts the opposite effect for cationic nanoparticles. This was validated by allowing cationic nanoparticles to bind to a DPPC membrane ($T_m \approx 40$ °C), which at the experimental temperature (≈20 °C) displayed $P \approx 0.6$ before nanoparticles were added. As shown in Fig. 2*D*, the net polarization then decreased, and detailed inspection of the emission raw data shows that the shift of emission wavelength was less pronounced than after adding carboxyl-modified nanoparticles to DLPC membrane as shown in Fig. 2*B*, consistent with the expected weaker binding of cationic particles (19). The decrease of *P* again suggests that the phase transition was localized to regions where nanoparticles had bound. In Fig. 2*D*, the final fraction of liquid phase can be estimated as 20%—although the experimental temperature was less than the literature value of this lipid's T_m. The addition of cationic nanoparticles to DLPC ($T_m \approx -1$ °C) liposomes induced negligible

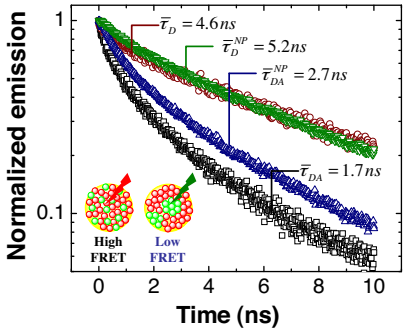

Fig. 3. Fluorescence emission plotted against time on the nanosecond time scale for FRET (Förster resonance energy transfer) experiments involving 200-nm DOPC liposomes after adding anionic (carboxyl-modified) nanoparticles at number ratio of particles to liposomes $C_{NP}/C_L = 200$. The fluorescence donor was NBD-DPPE (0.1% concentration) and the acceptor was RhB-DOPE (0.5% concentration). The mean lifetime of the donor increases, after nanoparticle binding, from 4.6 to 5.2 ns, and the FRET efficiency, evaluated from lifetime, decreases from 0.65 ± 0.06 to 0.45 ± 0.05. Alternatively, the *SI Text* shows fits of the fluorescence lifetimes to a sum of several decay processes. Wherever present in this figure, the superscript NP denotes the presence of bound nanoparticles, and the subscripts D and A refer to the presence of donor and acceptor fluorescent dyes, respectively. In the *Inset*, a schematic diagram compares randomly mixed FRET pairs, which is the situation of higher FRET efficiency, with the situation where the donor dye partitions into gel-phase regions as occurs in these experiments.

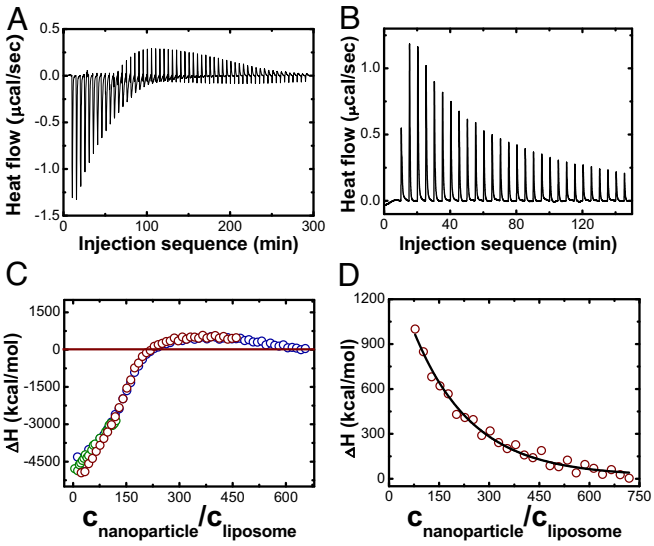

Fig. 4. Isothermal titration calorimetry of liposomes with nanoparticles added. (*A*) Raw data, heat flow plotted against injection sequence, when a fluid-phase 200-nm DLPC liposome suspension is exposed to increasing amounts of anionic nanoparticles as described in the text. (*B*) Raw data when a gel-phase 200-nm DPPC liposome suspension is exposed to increasing amounts of cationic nanoparticles. (*C*) Integrated enthalpy change after subtraction of heat of dilution plotted against number ratio of particles to liposomes, C_{NP}/C_L, for the case illustrated in *A*. Data obtained from different concentrations of injected particle suspension are shown in a color-coded manner: blue, 3 μM; red, 2 μM; and green,1 μM. The liposome concentration was fixed at 1 nM. (*D*) Integrated enthalpy change after subtraction of heat of dilution plotted against number ratio of particles to liposomes, C_{NP}/C_L, for the case illustrated in *B*. The heat of dilution was measured in separate control experiments and was subtracted for calculation of these binding isotherms.

change of net polarization, consistent with the anticipation that positively charged particles do not fluidize initially fluid lipids.

FRET experiments afforded an independent test of the hypothesis of nanoparticle-induced gelation, because the efficiency of energy transfer between 2 fluorescent dyes must decrease when they become spatially separated by partitioning into different phases. For this purpose, NBD and Rhodamine B (RhB) were selected because phospholipids bearing an NBD probe are known to partition into the gel phase of lipid membranes, but phospholipids bearing a RhB probe do not (21). Fig. 3 plots the logarithmic normalized emission against time on the nanosecond time scale under the conditions specified in the figure legend. The lifetime of NBD increased as anticipated after adding nanoparticles, consistent with its partitioning into the gel phase. In addition, the FRET efficiency in lifetime experiments decreased, indicating increased distances between the 2 dyes, as should be expected since the donor and acceptor dyes partitioned into different lipid phases. The magnitude of decrease is in the range expected from prior studies on microscopic phase separation involving 2 chemically different lipid components (21), corroborating the idea of local phase transition. The absolute value of the observed FRET efficiency shows that the domain size is in the range of 10–100 nm, according to theoretical estimates (22).

A final independent test of the hypothesis of nanoparticle-induced surface reconstruction consisted in using isothermal titration calorimetry (ITC) to measure the enthalpy (ΔH) of binding (23). Fig. 4*A* shows raw data when anionic nanoparticles were added to DLPC liposomes, and Fig. 4*C* shows the integrated heat change plotted against normalized nanoparticle concentration. Consistent with the hypothesis of nanoparticle-induced gelation, the initially exothermic binding was followed, at the highest NP concentrations, by an endothermic process, which is expected because binding-induced shrinkage of the liposome should be endothermic. Fitting gives the binding constant of $\approx 10^8\ M^{-1}$, corresponding to a modest free energy of binding, $\approx 20\ k_BT$ per particle. The dramatic difference between enthalpy and free energy reveals a significant contribution from entropy, presumably partly from loss of entropy by gelation, partly from release of hydrated water from the PC head groups when nanoparticles bind. The deviation of the fitting in the range of high molar ratio may reflect cooperative gelation, which also reconciles the absence of plateau in heat change with linearity of the phase transition measured by fluorescence polarization. But in contrast to this, allowing positively charged nanoparticles to bind to gel-phase DPPC liposomes showed that this process was uniformly endothermic, as anticipated if nanoparticles caused the lipids to fluidify. The raw data (Fig. 4*B*) was integrated to give the integrated heat change plotted against normalized nanoparticle concentration in Fig. 4*D*. Thus, the sign of calorimetric heat changes is consistent with the conclusions that emerged from the independent fluorescence measurements. We speculate that cooperativity of this fluidization may be less than of the gelation transition, which may be facilitated by long-range correlations of lipid chain alignment, but no quantitative explanation is presented at this time.

The traditional notion of how to produce spatially patchy stiffness of a phospholipid membrane is by phase separation of lipids with different intrinsic stiffness (10); but when phospholipid membranes reconstruct locally in response to binding as described here, it is reasonable to infer that they will be locally stiffer in the gelled patches and less stiff in the fluidized patches, so nanoparticle-induced reconstruction of the phase state offers a new mechanism to modulate stiffness. Similarly, the traditional notion of how to produce a thermodynamic line tension in a phospholipid membrane is from the phase coexistence of different components (24); this article, showing that even the same lipid can coexist in 2 different phases according to what binds to it, presents an additional mechanism. Binding-induced structural reorganization also provides a potential mechanism to couple

membrane fluctuation and transportation/clustering of absorbates (25). Surfactants are known to reorganize upon transfer to planar solids and removal from water (26), and it is intriguing to notice some analogy to the present very different case of in situ adsorption of nanosized particles. Also pleasing is to generalize the notion of environmentally induced surface reconstruction, which is prominent for metals and semiconductors (11–13) but not identified previously for phospholipid systems. However, it is worth emphasizing that as model phospholipid systems were studied here to simplify the problem, the question of generalizing the conclusions of this study to living organisms remains unresolved.

Materials and Methods

Materials. The phospholipids DLPC (dilauryl PC), DOPC (dioleoyl PC), and DPPC (dipalmitoyl PC) were obtained from Avanti Polar Lipids. Large unilamellar lipid vesicles were prepared at 1 vol% concentration in PBS buffer (10 mM; pH, 6.0) by the well-known extrusion method, employing procedures described in detail in ref. 18. Carboxyl-modified (negatively charged) and amidine-modified (positively charged) white polystyrene (PS) latex with a diameter of 20 nm were purchased from Interfacial Dynamics. In control experiments, silicon dioxide nanoparticles with diameters of 4, 10, or 20 nm were obtained from Alfa Aesar. Plasmids (4 kbp) with a radius gyration of ≈10 nm were extracted from *Escherichia coli* by using standard protocols. Charged nanoparticles were mixed by vortex into the liposome suspension at the desired molar ratio (18). From data given by the manufacturers, the surface charge density was calculated to be 1 charge per ≈1.1 nm^2 for carboxyl-modified polystyrene nanoparticles, ≈9 nm^2 for silica particles, and ≈4.0 nm^2 for amidine-modified nanoparticles.

The fluorescent dye Laurdan, 6-dodecanoyl-2-dimethylaminonaphthalene, was purchased from Molecular Probes. The FRET pair, *N*-(7-nitrobenz-2-oxa-1,3-diazol-4-yl)-dipalmitoylphosphatidylethanolamine) (NBD-DPPE) and *N*-(lissamine-rhodamine B)-dioleoylphosphatidylethanolamine (RhB-DOPE), were purchased from the same company.

Fluorescence Correlation Spectroscopy (FCS). FCS measurements were carried out in the 2-photon excitation mode by using a home-built apparatus. Briefly, a near-infrared femtosecond-pulse laser was focused onto the sample through an objective lens. The excitation spot had a diffraction-limited diameter of ≈0.35 μm. Fluorescence was collected and detected by a single-photon counting module. The translational diffusion coefficients (D) were obtained by fitting the fluorescence intensity–intensity autocorrelation function. The mean diameters of the liposomes, present at dilute concentration, were related to D by using the Stokes–Einstein equation (Fig. S1).

Dye Orientation Within Liposomes. The final concentrations of Laurdan and phospholipid were 0.8 μM and 0.4 mM, respectively (probe/phospholipid = 1:500). Steady-state emission spectra of Laurdan were measured by using a fluorometer (Photon Technologies) at magic angle condition with excitation at 340 nm. Emission spectra were corrected for instrument response. The characteristic wavelengths for gel and fluid phases, respectively, for various lipids were determined from the samples below or above the phase transition temperatures and agree with the values reported in the literature (27, 28).

FRET Experiments. The approach of measuring fluorescence lifetime was used to make time-resolved FRET measurements. The donor was NBD-DPPE (probe/phospholipid = 1:1,000), the acceptor was RhB-DOPE (probe/phospholipid = 1:200), in liposomes with 200 nm mean diameter. Excitation, achieved by a frequency-doubled Ti:sapphire laser, was performed at 460 nm to minimize RhB excitation and emission was measured in the region 500–530 nm, which selectively characterize NBD emission. The time-resolved lifetimes were measured by using a data acquisition board purchased from Becker & Hickl. Because the fluorescence lifetimes did not follow single-exponential kinetics, the mean lifetime was defined, in the conventional way (21), as $\bar{\tau} = \sum_i \alpha_i \tau_i$. In most cases, the data were fitted with second order exponential decays summarized in Table S1.

Isothermal Titration Calorimetry (ITC). Isothermal titration calorimetry was performed by using the VP-ITC high-sensitivity titration calorimeter (MicroCal) housed in the Post Genomics Institute at the University of Illinois. Typically, 58 consecutive aliquots of 5 μL each (for anionic PS particles), or 29 consecutive aliquots of 10 μL each (for cationic PS particles), containing nanoparticles at a concentration of 3 μM, were injected into the cell (1.43 mL) filled with 0.4 mM lipid solution (1 nM liposome). Both liposome and nanoparticle solutions were degassed under vacuum for 30 min immediately before use. Injections were made at 5-min intervals and at 0.5 $\mu L \cdot s^{-1}$ rate. A constant stirring speed of 300 rpm was maintained during the experiments to ensure sufficient mixing after each injection. For calculation of the binding isotherm, the heat of dilution was measured in separate nanoparticle-buffer titrations and was subtracted. Surface coverage was estimated from the raw data as follows. First, the projected nanoparticle area showed complete surface coverage in hexagonal close packing to occur at $C_{NP}/C_L = 400$; this estimate presents an upper bound of surface coverage. Second, $C_{NP}/C_L = 300$ is the point up to which changes of net polarization (P) were linear; therefore, the linear region in Fig. 2*C* ends at a fractional surface coverage of at least 0.75. Third, the calorimetry experiments showed that heat changes were completed approximately $C_{NP}/C_L = 500$. Assuming the binding affinity is still constant in the range of molar ratio between 300–500, but weaker because of electrostatic repulsion, we were able to extrapolate the surface coverage, and found out the relation of P to surface coverage remained linear in the whole range. We should mention that the surface coverage is estimated on the strong assumption that no cooperativity of phase transition exists, which cannot strictly be true but provides meaningful physical insight into the situation and quickly affords comparison between different systems, which would be difficult to achieve otherwise.

ACKNOWLEDGMENTS. We thank Janet S. Wong and Mo Jiang for experimental help. This work was supported by the U.S. Department of Energy, Division of Materials Science, under Award DEFG02-02ER46019. L.Z. acknowledges assistance through the Water CAMPWS, a Science and Technology Center of Advanced Materials for the Purification of Water [National Science Foundation (NSF) Grants CTS-0120978], as well as NSF Grant DMR 0605947 and NSF (Nanoscale Interdisciplinary Research Team) Grant CBET 060978.

1. Groves JT, Boxer SG (2002) Micropattern formation in supported lipid membranes. *Acc Chem Res* 35:149–157.
2. Daniel S, Albertorio F, Cremer PS (2006) Making lipid membranes rough, tough and ready to hit the road. *MRS Bull* 31:536–540.
3. Römer W, *et al.* (2007) Shiga toxin induces tubular membrane invaginations for its uptake into cells. *Nature* 450:670–675.
4. Fielding CJ, ed (2006). *Lipid Rafts and Caveolae* (Wiley-VCH, Weinheim, Germany).
5. Anderson RG, Jacobson KA (2002) Role for lipid shells in targeting proteins to caveolae, rafts, and other lipid domains. *Science* 296:1821–1825.
6. Simons K, Ikonen E (1997) Functional rafts in cell membranes. *Nature* 387:569–572.
7. Collins MD, Keller SL (2008) Tuning lipid mixtures to induce or suppress domain formation across leaflets of unsupported asymmetric bilayers. *Proc Natl Acad Sci USA* 105:124–128.
8. Forstner MB, Yee CK, Parikh AN, Groves JT (2006) Lipid lateral mobility and membrane phase structure modulation by protein binding. *J Am Chem Soc* 128:15221–15227.
9. Binder WH, Barragan V, Menger FM (2003) Domains and rafts in lipid membranes. *Angew Chem Int Ed* 42:5802–5827.
10. Baumgart T, Hess ST, Webb WW (2003) Imaging coexisting fluid domains in biomembrane models coupling curvature and line tension. *Nature* 425:821–824.
11. Billinge SJL (2007) The problem of determining atomic structure at the nanoscale. *Science* 316:561–565.
12. Somorjai GA, Contreras AM, Montano M, Rioux RM (2006) Clusters, surfaces, and catalysis. *Proc Natl Acad Sci USA* 103:10577–10583.
13. Zhang H, Gilbert B, Huang F, Banfield JF (2003) Water-driven transformation in nanoparticles at room temperature. *Nature* 424:1025–1029.
14. Dobrovolskaia MA, Mcneil SE (2007) Immunological properties of engineered nanomaterials. *Nat Nanotechnol* 2:469–478.
15. Nel A, Xia T, Mädler L, Li N (2006) Toxic potential of materials at the nanolevel. *Science* 311:622–627.
16. Somerharju P, Virtanen JA, Cheng KH (1999) Lateral organisation of membrane lipids—The superlattice view. *Biochim Biophys Acta Mol Cell Biol Lipids* 1440:32–48.
17. Cevc G, Marsh D (1987) *Phospholipid Bilayers: Physical Principles and Models* (Wiley, New York).
18. Zhang LF, Granick S (2006) How to stabilize phospholipid liposomes (using nanoparticles). *Nano Lett* 6:694–698.
19. Yu Y, Anthony SM, Zhang LF, Bae SC, Granick S (2007) Cationic nanoparticles stabilize zwitterionic liposomes better than anionic ones. *J Phys Chem C* 111:8233–8236.
20. Gaus K, *et al.* (2003) Visualizing lipid structure and raft domains in living cells with two-photon microscopy. *Proc Natl Acad Sci USA* 100:15554–15559.
21. de Almeida RDF, Loura LMS, Fedorov A, Prieto M (2005) Lipid rafts have different sizes depending on membrane composition: A time-resolved fluorescence resonance energy transfer study. *J Mol Bol* 346:1109–1120.
22. Towles KB, Dan N (2007) Determination of membrane domain size by fluorescence resonance energy transfer: Effects of domain polydispersity and packing. *Langmuir* 23:4737–4739.

23. Cedervall T, *et al.* (2007) Understanding the nanoparticle-protein corona using methods to quantify exchange rates and affinities of proteins for nanoparticles. *Proc Natl Acad Sci USA* 104:2050–2055.
24. Kuzmin PI, Akimov SA, Chizmadzhev YA, Zimmerberg J, Cohen FS (2005) Line tension and interaction energies of membrane rafts calculated from lipid splay and tilt. *Biophys J* 82:1120–1133.
25. Reynwar BJ, *et al.* (2007) Aggregation and vesiculation of membrane proteins by curvature-mediated interactions. *Nature* 447:461–464.
26. Yaminsky V, Nylander T, Ninham B (1997) Thermodynamics of transfer of amphiphiles between the liquid-air interface and a solid surface-wetting tension study of Langmuir–Blodgett films. *Langmuir* 13:1746–1757.
27. Parasassi T, De Stasio G, Ravagnan G, Rusch RM, Gratton E (1991) Quantitation of lipid phases in phospholipid-vesicles by the generalized polarization of Laurdan fluorescence. *Biophys J* 60:179–189.
28. De Vequi-Suplicy CC, Benatti CR, Lamy MT (2006) Laurdan in fluid bilayers: Position and structural sensitivity. *J Fluorescence* 16:431–439.